Sensors & Diagnostics

PAPER

View Article Online
View Journal | View Issue

Cite this: *Sens. Diagn.*, 2024, **3**, 1533

3D-printed electrochemical cells for multi-point aptamer-based drug measurements†

John Mack, [a] Raygan Murray,[a] Kenedi Lynch[b] and Netzahualcóyotl Arroyo-Currás *[ac]

Electrochemical aptamer-based (E-AB) sensors achieve detection and quantitation of biomedically relevant targets such as small molecule drugs and protein biomarkers in biological samples. E-ABs are usually fabricated on commercially available macroelectrodes which, although functional for rapid sensor prototyping, can be costly and are not compatible with the microliter sample volumes typically available in biorepositories for clinical validation studies. Seeking to develop a multi-point sensing platform for sensor validation in sample volumes characteristic of clinical studies, we report a protocol for in-house assembly of 3D-printed E-ABs. We employed a commercially available 3D stereolithographic printer (FormLabs, $5k USD) for electrochemical cell fabrication and directly embedded electrodes within the 3D-printed cell structure. This approach offers a reproducible and reusable electrode fabrication process resulting in four independent and simultaneous measurements for statistically weighted results. We demonstrate compatibility with aptamer sequences binding antibiotics and antineoplastic agents. We also demonstrate a proof-of-concept validation of serum vancomycin measurements using clinical samples. Our results demonstrate that 3D-printing can be used in conjunction with E-ABs for accessible, rapid, and statistically meaningful validation of E-AB sensors in biological matrices.

Received 7th June 2024,
Accepted 3rd August 2024

DOI: 10.1039/d4sd00192c

rsc.li/sensors

1. Introduction

Electrochemical aptamer-based (E-AB) sensors are platforms that allow reagentless detection and quantitation of biomedically relevant analytes in biological fluids. For example, E-AB sensors have been developed for the antibiotic vancomycin,[1] the cell signaling marker platelet-derived growth factor (PDGF),[2] and the potential biomarker of renal injury neutrophil gelatinase-associated lipocalin (NGAL).[3] However, while a large amount of cutting-edge work is being done in the E-AB sensor space, the sensors are typically fabricated on commercially available single-channel electrodes, which must be purchased from specialty vendors. These electrodes are costly and bulky, precluding their implementation in clinical validation studies that necessitate sub-milliliter sample volumes. The result is E-AB sensor development studies that often do not report rigorous power analyses nor statistically weighted data[4] to support effective clinical validation of their potential biomedical or diagnostic application.

Customizing electrodes for multichannel E-AB sensing at scale and with a form factor that can support measurements in the sub-milliliter volumes of clinical samples can be achieved *via* manufacturing strategies such as lithography or screen printing. Lithographic techniques produce excellent, geometry-controlled substrates for E-AB sensing but are costly and require access to specialized equipment, including cleanroom facilities.[5] Screen printing strategies, in contrast, are cost-efficient and scalable but do not always produce electrodes with the quality needed for reproducible E-AB sensing. Specifically, control over the aptamer monolayer density in E-AB sensors is required to achieve reproducible signaling gain. Yet, aptamer density is a strong function of surface quality and gold purity, which may significantly vary across screen-printed electrode batches.[6,7] Thus, lithography and screen-printing methods are manufacturing strategies that require considerable specialization to (1) have access to the instrumentation needed and (2) achieve reproducible manufacturing, limiting their broad adoption in the field of E-AB sensing.

One alternative for overcoming this roadblock is the use of additive manufacturing techniques, such as 3D-printing, for rapid prototyping and production of multiplexed electrode

[a] *Biochemistry, Cellular and Molecular Biology Program, Johns Hopkins University School of Medicine, 316 Hunterian Building, 725 North Wolfe Street, Baltimore, MD 21205, USA. E-mail: netzarroyo@jhmi.edu; Tel: +1 443 287 4798*
[b] *Amgen Scholars Program, Krieger School of Arts and Sciences, Johns Hopkins University, Baltimore, MD 21218, USA*
[c] *Department of Pharmacology and Molecular Sciences, Johns Hopkins University School of Medicine, Baltimore, MD 21205, USA*

† Electronic supplementary information (ESI) available. See DOI: https://doi.org/10.1039/d4sd00192c

arrays.[8,9] The versatile nature of 3D-printing design, as well as the rise in accessibility of 3D-printing technology in recent years, makes it the ideal modality for rapid E-AB development and analytical validation.[10,11] Electrochemical cells with the desired dimensions and electrode count can be designed, printed, and assembled quickly and at relatively low cost. Shape, volume, and electrode number can be easily adapted for changes in user needs as prototyping is ongoing. Motivated by this versatility, here we present a protocol for the cost-effective manufacture of stereolithographically 3D-printed electrochemical cells, equipped with four gold working electrodes, one counter electrode, and one reference electrode. These "plug-and-play" type cells can directly be used with common laboratory potentiostats to function as self-contained units for the fabrication and analytical validation of E-AB sensors. Their chambers are designed to hold between 75 and 300 μLs of volume, which is compatible with sample volumes available from biorepositories.[12] Their multichannel format allows for statistical redundancy in molecular measurements to support rigorous validation studies. We show that these 3D-printed cells are reusable, can be effectively functionalized with a variety of aptamers, and support measurements in complex biological matrices such as undiluted human serum.

2. Methods

Materials and reagents

Alkylthiol (3′) and methylene blue (MB, 5′)-modified DNA aptamer sequences (Table 1) were purchased from Integrated DNA Technologies (Coralville, IA). Gender-pooled, de-identified, human serum was purchased from Bio IVT (New York, USA). >99.8% ethanol, >96.5% mercaptohexanol/MCH, tris-(2-carboxyethyl) phosphine hydrochloride (TCEP, >98%), sodium chloride (NaCl, >99.5%), potassium chloride (KCl, >99%), magnesium chloride (MgCl2, >99%), and calcium chloride (CaCl2, >99%), vancomycin hydrochloride, tobramycin sulphate, procaine, and irinotecan were purchased from Sigma Aldrich. All stock solutions were dissolved in either ultrapure water or gender-pooled human serum (HUMANSRM-9909-D, BioIVT).

3D-printed device construction

All three cell components ("shell", "chamber ring", and "backing") were printed using a Formlabs 3B+ 3D printer using High Temp Resin (FormLabs, Sommerville, MA). After completion, prints were removed from the printer and rinsed for ~10 minutes in isopropyl alcohol. After rinsing, four 0.5 mm diameter gold wires (010966.BY, Thermo Fisher Scientific, USA), one 0.25 mm diameter silver wire (7440-22-4, Alfa Aesar, Ward Hill MA), and one 0.5 mm diameter platinum wire were individually soldered to breakout cables and embedded in the corresponding holes in the shell (Fig. S1†), such that approximately 0.5 mm of wire was exposed on the front of the shell. More resin was used to seal the wiring in place, then the prints were UV-cured at 80 ° C for 2 h using a Form Cure (FH-CU-01, Formlabs, Sommerville MA). After curing, the exposed wire was trimmed down and the front surface was hand-polished smooth with 30 μm, 15 μm, 9 μm, 3 μm, 2 μm, and 1 μm aluminum oxide/silicon carbide polishing paper (37-948, Zona Tool Co., Bethel, CT), then cured again. The lid was fitted with an O-ring in the central notch; the lid and the backing were cured as mentioned above.

Commercial macroelectrode E-AB preparation

The electrode surface was polished on a wetted cloth polishing pad (MF-1040, BASi, West Lafayette, IN) with MetaDi™ 1 μm (40-6630, Buehler, Lake Bluff, IL) and MetaDi™ 0.1 μm (40-628, Buehler, Lake Bluff, IL) polycrystalline diamond suspension, followed by alumina slurry (CF-1050, BASi, West Lafayette, IN). Following mechanical cleaning, the electrodes were cleaned electrochemically by scanning 500 times while mixing in cyclic voltammetry mode at 1 V s^{-1} in 0.5 M NaOH, from −0.6 V to −1.8 V *vs.* Ag/AgCl. Electrodes were then transferred to 0.5 M H_2SO_4 and scanned 5 times at 0.5 V s^{-1} from 0.4 V to 1.7 V *vs.* Ag/AgCl. Immediately after the last cycle, the 0.5 M H_2SO_4 was removed and replaced with 0.05 M H_2SO_4, and one CV scan was measured from 0.4 V to 1.65 V at 0.1 V s^{-1}. Electrodes were immediately rinsed with DI water and purged with nitrogen gas. For electrode functionalization, DNA aptamer was mixed with 10 mM tris(2-carboxyethyl) phosphine (TCEP) at a 1 : 1 ratio, incubated for one hour at room temperature, then diluted to the desired deposition concentration. Freshly cleaned electrodes were immersed in the reduced and diluted aptamer, and incubated for 1 hour at 4 °C. The electrodes were then transferred to 1 mM 6-mercapto-1-hexanol (MCH) solution and incubated overnight at room temperature.

3D-printed device E-AB preparation

Immediately prior to fabrication with E-AB sensors, the device surface was polished using the diamond/alumina polishing protocol mentioned above. The device was then assembled, and the chamber filled with 200 μL of 0.5 M s NaOH. The electrodes were then electrochemically cleaned by cyclic voltammetry, scanning at 1 V s^{-1} from −0.4 V to −1.6 V *vs.* Ag for 500 scans, replacing the NaOH every 100 scans. The

Table 1 DNA aptamer sequences

Name	Sequence
Tobramycin[13]	5′-GGC GAC AAG GAA AAT CCT TCA ACG AAG GTG GGT GGC C-3′
Vancomycin[1]	5′-CGA GGG TAC CGC AAT AGT ACT TAT TGT TCG CCT ATT GTG GGT CGG-3′
L-Procaine[14]	5′-GGC GAC AAG GAA AAT CCT TCA ACG AAG GTG GGT GGC C-3′
Irinotecan[11]	Proprietary (Aptamer Group, York, UK)

chamber was briefly rinsed then filled with 200 μL of 0.5 M H_2SO_4, and scanned 5 times from 0.3 V to 1.4 V *vs.* Ag at 0.5 V s^{-1}. For the roughened electrodes (Fig. 6 and S5 and S6†), the electrodes were then subjected to chronoamperometry, alternating the potential between 0 V to 2 V for 16 000 cycles, with continuous mixing by pipetting and replacing the 0.5 M H_2SO_4 every 4000 cycles. Finally, the chamber was rinsed and filled with 200 μL of 0.05 M H_2SO_4 and scanned between 0.3 V and 1.4 V *vs.* Ag once. The chamber was immediately rinsed with water and filled with 100 μL DNA aptamer solution, which had been reduced for 1 hour at room temperature with a 1 : 1 ratio of TCEP then diluted to the desired deposition concentration. Parafilm was used to seal the chamber and the device was incubated at 4 °C for 1 hour, after which the aptamer solution was removed and replaced with 150 μL 1 mM MCH. The chamber was sealed again with parafilm and incubated overnight at room temperature.

E-AB measurement protocol

Electrochemical measurements were carried out using a CH Instruments Model 1040C electrochemical analyzer (CH Instruments, Austin, TX). Cyclic voltammetry measurements were performed using a 1 mV scan interval with 2 s of quiet time, and square wave voltammetry measurements were performed using a square wave amplitude of 25 mV, and step increments of 1 mV for frequencies >100 Hz and 5 mV for frequencies ≤100 Hz.

Packing density quantification

To determine the density of aptamer probes on the electrode surface, we first calculated the real area of each bare electrode by recording the integrated current of the gold oxide reduction peak for the final CV scan in 0.05 M H_2SO_4, then dividing by the reported value of charge consumed by the reduction of gold oxide per square centimeter (400 μC cm^{-2}). The electrode was then functionalized as described and scanned at three different CV scanning frequencies prior to other experiments being performed. The average integrated current for these three frequencies (Q) was input alongside the real electrode area (A) into the following equation, where Γ represents the probe concentration in 10^{12} probes per cm^2 and F is Faraday's constant, assuming two electrons transferred per molecule of methylene blue:

$$\Gamma = Q/(2FA) \quad (1)$$

E-AB sensor frequency mapping

Frequency maps were generated by scanning E-AB sensors in buffer with square wave voltammetry at increasing frequencies from 5 Hz to 1000 Hz. A saturating concentration of target was then added to the buffer, and the sensors scanned again. The integrated current of the resulting peaks (*i.e.* the charge transferred) was then plotted as a function of frequency.

E-AB sensor calibration

All sensors presented here were calibrated by titration with increasing concentrations of analyte in either phosphate buffer or human serum, scanning with square wave voltammetry (SWV) at two different frequencies selected from frequency maps for signal-on and signal-off behavior. For calibration curves, a simplified kinetic differential measurement (KDM) was calculated by subtracting signal-on peak current normalized to the first titration point, from signal-off peak current normalized to the first titration point. This value, referred to as gain, was then plotted as a function of target concentration and fit to the Hill equation (eqn (2)):

$$\text{gain} = \text{base} + \{(\text{max} - \text{base})/(1 + (EC_{50}/[\text{target}])^{\text{rate}})\} \quad (2)$$

Base represents the curve baseline, max represents the curve maximum, [target] is the target concentration, and rate is the Hill coefficient. The resulting thermodynamic constants derived from the nonlinear regression of these data to eqn (2) were used in subsequent calculations. Values of the constants were left unconstrained for the fit calculation, unless otherwise specified.

3D-printed device sample quantification

To estimate sample concentration of vancomycin, signal gain was recorded by scanning with SWV at 5 Hz and 300 Hz or 30 Hz and 300 Hz, and subtracting the peak currents as described above, normalized to a scan with blank serum. The device was used 5 times serially, rinsed with either blank serum or 4 M urea between each measurement, and a scan in blank serum taken prior to the next measurement. No significant difference was observed between wash protocols using either blank serum or urea. Example peak currents serially measured in serum alternating between the presence and absence of target are included in Fig. S7.† The concentration value for each sample was calculated by entering the calculated gain into eqn (2), along with the thermodynamic parameters derived from the nonlinear regression of the calibration data taken from the sensor on that day and solving for [target].

Sample collection and automated immunoassay sample preparation and measurement

The clinical samples employed in this work were collected with informed consent from patients being treated at the Johns Hopkins Hospital. All measurements were performed in accordance with principles of the Declaration of Helsinki, the Good Clinical Practice guidelines of the International Council for Harmonization, and approved by the ethics committee at Johns Hopkins University, under protocol IRB00241649. After the specimens were subjected to their usual diagnostic assays, fluid remnants labeled to be discarded were retained, completely de-identified, and transferred to the JHH Point-of-Care Laboratory. The vancomycin concentration in such specimens was first determined *via* competitive immunoassays. Briefly, the samples were filtered by centrifugation with a Vivafree™ 2 filter (VFR02H23, Viva Products, Littleton, MA) at

4000 rpm for 20 minutes to remove serum proteins and protein-bound vancomycin. The Roche Cobas 502 automated chemistry analyzer was used to quantify serum vancomycin concentrations *via* the kinetic interaction of microparticles in solution (KIMS) assay, according to the manufacturer's protocol.

Data analysis and software

Peak current and charge values were extracted from raw voltametric data using SACMES, and open-source Python script package developed by our lab.[15] All data and data fits reported were plotted, analyzed, and graphically displayed using Igor Pro v8 (Wavemetrics, Lake Oswego, OR). For box plots, the center line represents the median, the box represents the interquartile range boundaries, and the whiskers represent maximum and minimum values. Linear and Hill equation fits were performed using Igor's native calculation packages. For Bland–Altman plots, the 95% confidence interval (CI) was determined with eqn (3).

$$\text{Mean} \pm (1.96 \times \text{Standard Deviation}) \quad (3)$$

3. Results and discussion

The first objective of this study was to prototype an electrochemical cell that could hold a 75–300 μL volume of clinical sample[12] while also allowing for redundant E-AB measurements within that sample (Fig. 1). To construct such a cell, we designed and stereolithographycally printed a cross-shaped body with six apertures 550 μm in diameter (Fig. 1A). Separately, we soldered 3 mm-long segments of gold, platinum, and silver wires to the ends of insulated copper wire, and electrically insulated the joint with heat-shrink tubing. These wires were passed through the apertures in the 3D print such that ~1 mm of each wire was exposed on the other side (Fig. 1B). We sealed the wires in place by pipetting in extra resin and UV curing the device for 2 h at 80 °C (Fig. 1C). Once cured, we trimmed the wires and hand-polished the surface of the device uniformly to achieve a mirror finish on the flat disk electrodes (Fig. 1D). After polishing, we sandwiched the cross-shaped device between a 3D-printed brace and a 3D-printed chamber lid containing a rubber O-ring (Fig. 1E). Assembling the device with screws created a water-tight ~300 μL volume chamber (Fig. 1F). The resulting device was able to be repeatedly re-used by disassembling the three components, hand polishing the surface with 1 μm aluminum oxide/silicon carbide polishing paper, and performing electrochemical cleaning as indicated in the Methods. For example, one device used in this study has been polished and re-used over 50 times. The printing, curing, and polishing could be completed over the course of a single day, and multiple devices were printed at once. All 3D-printed parts were printed using a FormLabs 3B+ printer, using their commercial High Temp resin. A cost-comparison between cell components and purchased commercial macroelectrodes can be found in Table 2.

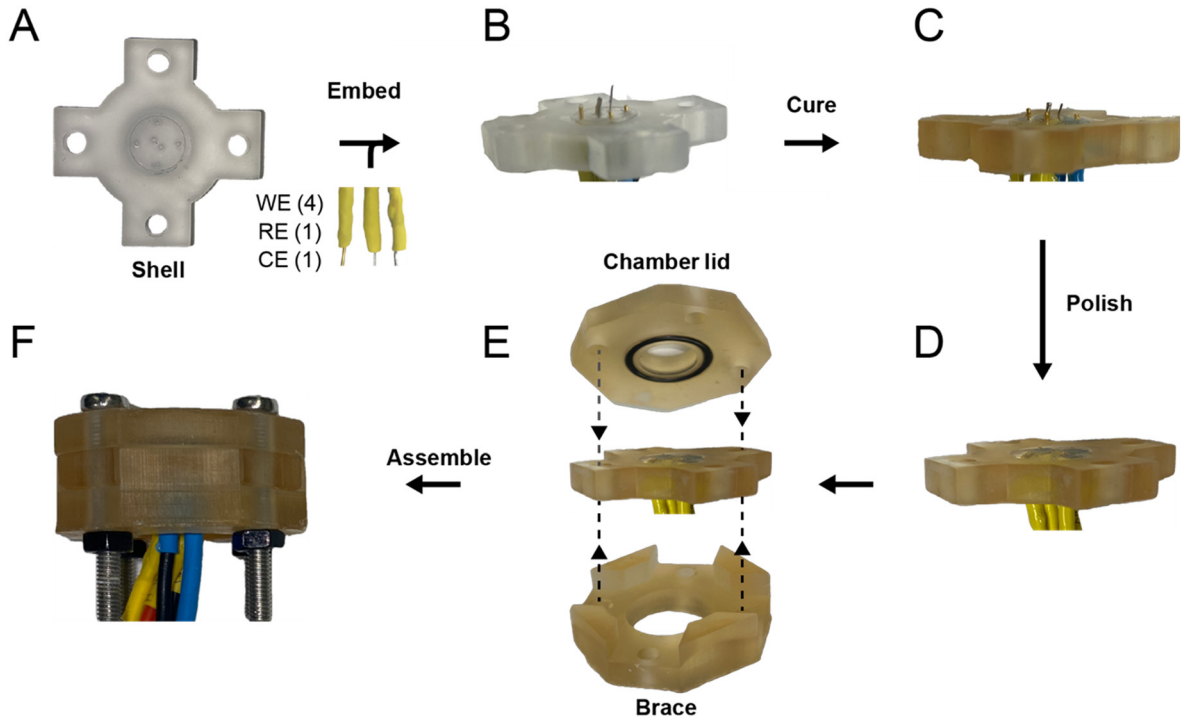

Fig. 1 Construction workflow for 3D-printed electrochemical cell. (A) The device shell, rinsed of any uncured resin. (B) Four gold working electrodes (WE), one silver pseudo-reference electrode (RE), and one counter electrode (CE) are made by soldering three-millimeter-long segments of the corresponding metal wire to insulated copper wire and physically embedding them into the 3D-printed shell. (C) The wires are cured in place with additional resin. (D) Wire ends are trimmed and manually sanded flush with the 3D-printed surface. (E) Separately printed lid and brace parts are screwed into place on either side of the electrode device. (F) The fully assembled device, ready to use.

Table 2 Cost breakdown of the proposed 3D-printed electrochemical cell, and comparison with commercially available macroelectrodes

Item	Supplier	Cost (USD)
3D-printing resin (7.5 mL)	Formlabs	$1.49
Gold wire (20 mm)	Fisher Scientific	$22.01
Platinum wire (5 mm)	Fisher Scientific	$8.83
Silver wire (5 mm)	Fisher Scientific	$0.03
Fully assembled 4-channel device	**Total:**	**$31.76**
2.0 mm macroelectrode	CH Instruments	$90
1.6 mm macroelectrode	CH Instruments	$305
1.6 mm macroelectrode	BASi	$210
3.0 mm macroelectrode	BASi	$350

The second objective of this study was to demonstrate that our 3D-printed electrochemical cell could be used for statistically redundant molecular measurements in biorepository-compatible biofluid volumes (typically ≤250 μL). For reference, standard commercial gold disk macroelectrodes (cME) (Fig. 2A) typically range between 1–3 mm in geometrical diameter of the disk electrode, plus ~2 mm of electrode insulation, and require pairing with external counter and reference electrodes. This footprint makes them incompatible with sample volumes below 250 μL if multiple electrodes are to be used for measurement redundancy. In contrast, our integrated electrochemical cell (Fig. 1F) consists of four gold disk working (W, 500 μm in diameter), one platinum counter (C, 500 μm in diameter), and one silver pseudo-reference (R, 250 um in diameter) electrodes embedded in a 3D-printed body (Fig. 2B). The cell is watertight and can accept 75–300 μL of biofluid sample.

After assembly, the embedded gold disk electrodes can be functionalized *via* incubation in solutions containing 3′ hexanethiol linker- and 5′ methylene blue (MB)-modified aptamers, and 6-mercapto-1-hexanol to form E-AB sensing monolayers (Fig. 2C). In the context of these monolayers, the rate of electron transfer from MB to the underlying gold electrodes is a function of target binding. When target is present, MB undergoes faster electron transfer, causing an increase in the sensor signal. In the absence of target, electron transfer from MB is slow, and the sensor output decreases in magnitude.[16] These effects were monitored *via* square wave voltammetry, which is a frequency-dependent technique. By mapping the square wave frequency space at constant amplitude and step size, we obtained frequency maps in which the maximum current qualitatively reflects the average rate of electron transfer (Fig. 2D and E). This rate increased (*i.e.*, shifts to the right relative to the *x*-axis) with increasing target concentrations. E-ABs fabricated on cMEs (Fig. 1D), or our 3D-printed cells (Fig. 1E) generated

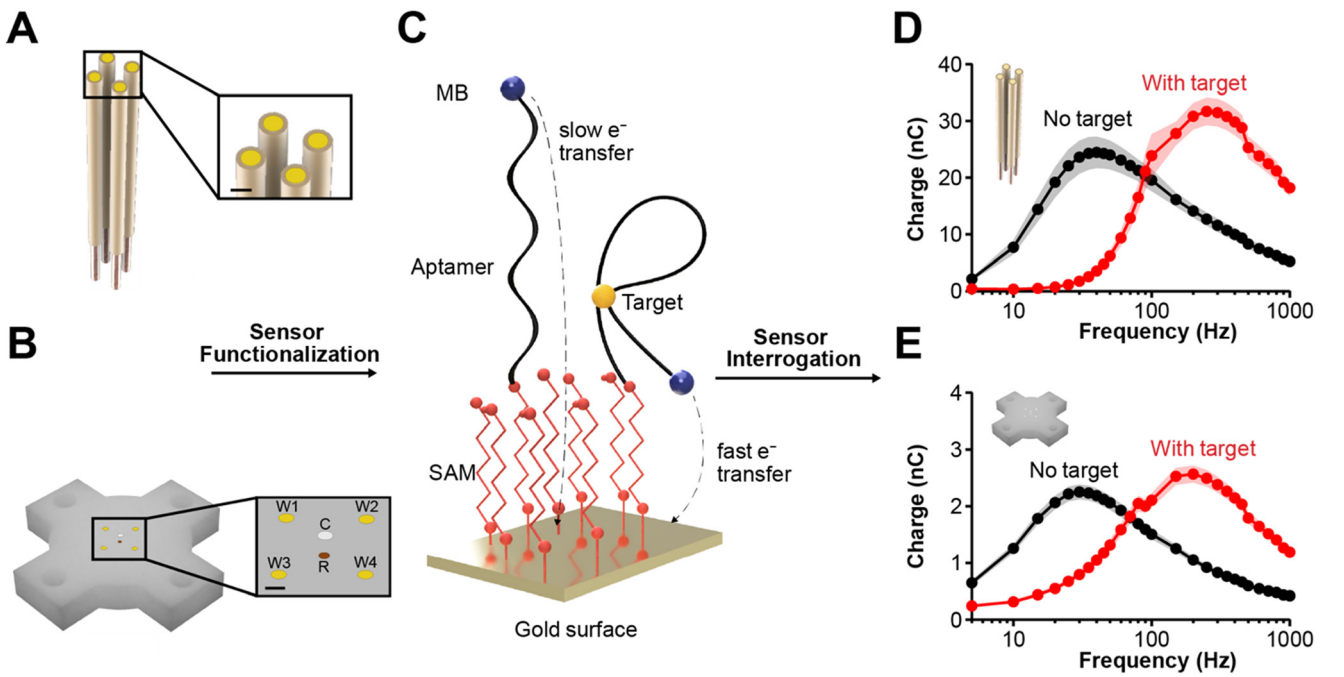

Fig. 2 Multipoint, 3D-printed electrochemical cells for redundant E-AB measurements in biofluids. (A) Digital rendering of four commercial macroelectrodes (cME), with inset magnifying gold electrode surface. Scale bar = 2 mm. (B) Digital rendering of the wire-embedded 3D-printed cell. The inset displays four gold working electrodes (W, yellow), one platinum counter (C, grey) and one silver reference (R, silver). Scale bar = 1 mm. (C) Schematic representation of the E-AB sensor architecture, with the gold electrode surface, a mercaptohexanol self-assembled monolayer (SAM), 5′ hexanethiol- and 3′ methylene blue (MB)-modified aptamer. Target (yellow sphere) binding to the aptamer causes a change in the electron transfer rate between the MB reporter and the underlying gold electrode. (D) Plot of charge transfer as a function of sampling frequency for cMEs functionalized using 200 nM tobramycin aptamer (final surface concentration = 8.7 ± 1.3 × 10^{11} molecules per cm^2), in the presence of 0 μM (black) or 500 μM (red) tobramycin in phosphate buffered saline. (E) Same as (D) but using the 3D-printed cell instead (final surface concentration = 3.7 ± 0.12 × 10^{11} molecules per cm^2). Points represent the average of n = 4 electrodes. Shaded regions represent standard deviation.

frequency maps with similar signal-to-noise output. However, the net current magnitude was lower in the case of the 3D-printed cell, which could be attributed to the microscopic surface area of its gold electrodes being smaller.

The 3D-printed electrochemical cells supported fabrication of E-AB sensors regardless of aptamer used. To illustrate this ability, we prepared 3D-printed devices using four different aptamer sequences, binding the aminoglycoside tobramycin (Fig. 3A),[13] the chemotherapeutic irinotecan (Fig. 3B),[11] the glycopeptide vancomycin (Fig. 3C),[1] and the analgesic procaine (Fig. 3D).[14] We tested the performance of the resulting E-AB sensors in a clinically relevant context by constructing dose–response curves of target molecules in undiluted human serum. Serum was selected because the clinical samples available for this study were preprocessed at the Johns Hopkins Hospital in accordance to their standard-of-care therapeutic drug monitoring protocols, which require serum for drug quantification. We challenged the sensors by monotonically increasing the concentration of their respective target. For each concentration measurement, the sensors were interrogated using square wave voltammetry at signal-on and signal-off frequencies, based on previously generated frequency maps (Fig. S2†). We performed nonlinear regression analyses of the resulting curves (Fig. 3) at each frequency using the Hill isotherm. The estimated EC_{50} for $signal_{on}$ and $signal_{off}$ for each curve is shown in Table 3, along reference values measured on macroelectrodes (cMEs data shown in Fig. S3†). Differences in EC_{50} between cMEs and our 3D printed devices are generally less than one order of magnitude and could be due to differences in the aptamer surface packing density between electrode types. Nevertheless, these results demonstrated the ability of the 3D-printed devices to support E-AB sensing irrespective of the aptamer employed, with signaling performance that positively compares against values measured using commercial electrodes.

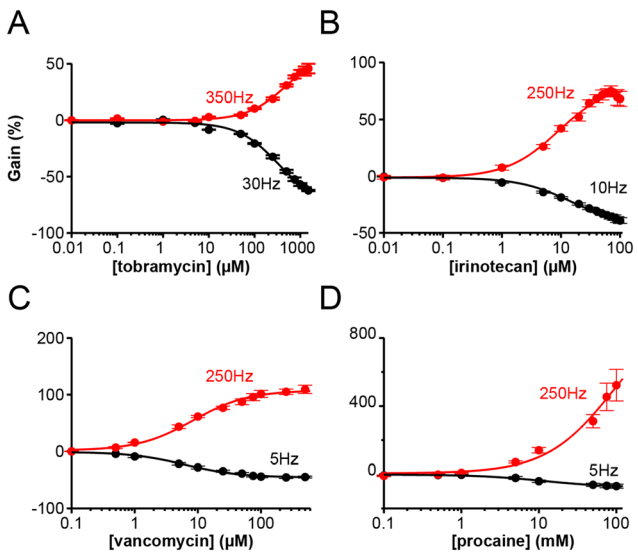

Fig. 3 E-AB sensor calibrations using 3D-printed devices. We generated signal-on (red) and off (black) dose–response curves for E-ABs using four different aptamer sequences binding (A) the aminoglycoside tobramycin, (B) the chemotherapeutic irinotecan, (C) the glycopeptide vancomycin, and (D) the analgesic procaine. Each solid marker represents the average of four electrodes contained in a single 3D-printed cell, and error bars represent the standard deviation. Solid lines represent non-linear regression fits to the Hill isotherm, assuming a binding coefficient of 1.

Table 3 Comparison of EC_{50} values between E-AB sensors on commercial macroelectrodes (cME) and 3D-printed electrochemical cells

Target	cME EC_{50}	3D printed device EC_{50}
Irinotecan	16.6 μM	10.3 μM
Procaine	6 mM	59.2 mM
Vancomycin	1.5 μM	7.7 μM
Tobramycin	236.8 μM	403.4 μM

Device-to-device E-AB sensing output in serum was reproducible to within 10% error. To assess this level of precision, we fabricated three independent 3D-printed cells on three independent days and functionalized them using a vancomycin aptamer sequence previously optimized by our group.[1] We deposited the aptamer from a 500 nM solution stock and back-filled the monolayer with 6-mercaptohexanol, achieving a surface concentration of $0.21 \pm 0.11 \times 10^{12}$ molecules per cm^2. We then challenged the sensors using vancomycin concentrations ranging from 0.1 to 500 μM in undiluted human serum, while interrogating using square wave voltammetry at signal-on (250 Hz) and signal-off (5 Hz) frequencies (the amplitude was constant at 25 mV and step size at 1 mV). Using the resulting data, we performed kinetic differential measurements (KDM) to eliminate drift in sensor signals by subtracting the relative sensor gain measured at 5 Hz from the one measured at 250 Hz. Fig. 4A shows the resulting sensor calibration curve in box plot format to better visualize the spread of the data and correlation coefficients. The error was propagated from the individual measurements as the square root of the sum of the relative standard deviations at signal-on and off responses. The resulting relative standard deviation was <9% at each concentration measurement across all devices/days. Finally, we performed nonlinear regression analysis of the average KDM trace to the Hill isotherm (Fig. 4B), resulting in an $EC_{50} = 7.4 \pm 0.9$. Overall, these results demonstrate that the proposed 3D-printed electrochemical cells supported highly precise E-AB measurements across independent fabrication batches and measurement days.

Next, we sought to assess the effectiveness of our 3D-printed cell device in the context of low volume bio-banked samples. To this end, a 3rd party prepared 120 simulated patient serum samples by spiking commercially purchased, gender-pooled human serum with known quantities of vancomycin between 0 and 40 μM. These samples were then encoded by the preparer, and not decoded until after data processing was complete. We used square wave voltammetry to measure the change in sensor current (*i.e.*, gain) for each sample relative to blank, vancomycin-free serum. The chamber was washed with 4 M urea between each measurement to regenerate the sensors (*i.e.*,

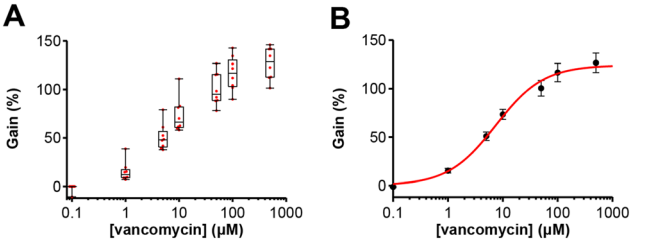

Fig. 4 Calibration of 3D-printed devices with vancomycin aptamer. (A) The difference in normalized peak current measured by square wave voltammetry between 250 Hz and 5 Hz as a function of concentration in undiluted, gender-pooled human serum. Each point represents the average current from three or four electrodes, the box represents the interquartile range of all points, while the upper and lower whiskers represent maxima and minima for each concentration value. Values exceeding 150% of the interquartile range are considered outliers. For all measurements n = 8 3D-printed devices were used. (B) Average KDM for all the sensors in (A) plotted as a function of vancomycin concentration. Red line represents a nonlinear regression fit to the Hill equation, assuming 1 : 1 binding and baseline = 0. Error bars represent standard deviation.

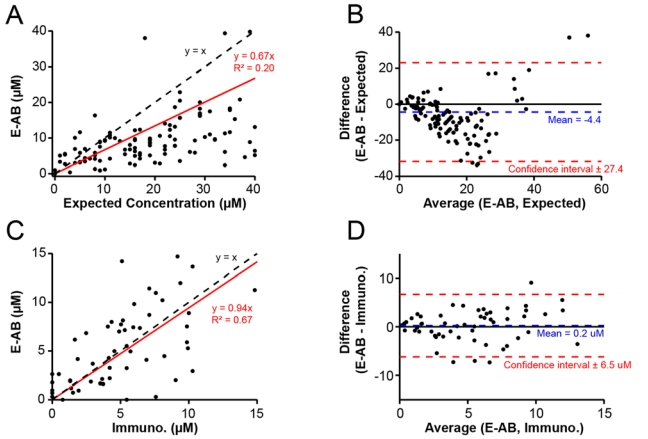

Fig. 5 Simulated patient sample and actual patient sample analysis using 3D-printed device. (A) Correlation between the vancomycin concentration calculated *via* E-AB sensor fabricated on the 3D-printed chamber device (*y*-axis) *versus* the expected concentration for simulated patient samples (*x*-axis) made using commercial serum spiked with vancomycin. (B) Bland–Altman plot of samples plotted in (A). (C) Correlation plot for actual patient samples, plotting concentrations calculated by E-AB sensors (*y*-axis) *versus* values calculated *via* competitive immunoassay (*x*-axis). (D) Bland–Altman plot for sample concentrations plotted in (C). Solid red lines represent linear regression of correlation data, with the *y*-intercept constrained to 0. The blue dashed lines represent the mean difference values, while the red dashed lines represent upper and lower bounds of the respective 95% confidence intervals.

to remove any serum proteins non-specifically bound to the sensor surface). We then fed the gain value of each measurement into the regression Hill equation from Fig. 4B, using the gain and EC_{50} derived from the data presented in that figure. This allowed us to solve for the unknown concentration value, outputting an estimated vancomycin concentration.

Once electrochemical measurements were complete, expected concentration values for each sample were decoded and compared to the electrochemically calculated value (Fig. 5A). The resulting values show mild correlation at known concentrations <10 μM; however, the E-AB sensors markedly underestimated the concentration of samples at expected concentrations exceeding approximately 10 μM. This behavior is further illustrated in a Bland–Altman plot[17] (Fig. 5B), which displays the difference between the calculated and expected values as a function of the average of the two values. As the average concentration value increases, the difference becomes more negative, suggesting that the sensor systemically underestimates the sample concentration at high vancomycin concentrations. Data from a prior publication from our group[1] suggests that, for the specific vancomycin aptamer sequence employed in this work, single-point measurements often generate lower signal gain than a corresponding concentration value in the context of a titration measurement, where the vancomycin concentration is serially increased point by point. Since calibration was done by challenging the sensor with gradually increasing vancomycin concentrations, this would explain the measurement discrepancy at higher concentrations.

To investigate how the 3D-printed electrochemical cells performed when used with real patient samples, we evaluated 54 vancomycin-containing patient plasma samples from a previously published clinical study.[18] The concentration range of such samples falls below the threshold where the sensor consistently underestimates the sample concentration, circumventing the issue discussed previously. For this second study, we measured the vancomycin concentration of sets of five different patient samples serially, by loading each sample into the same aptamer-modified, 3D-printed cell, interrogating the sensors, then washing with blank serum prior to the next sample. Signal recovery data following serial washing and interrogation is shown in Fig. S7.† Each sensor device was then challenged with commercially available serum spiked with increasing concentrations of vancomycin to obtain a calibration curve. The concentration of vancomycin in each patient sample was calculated based on the calibration curve collected at the end of each serial test. We then compared the results to the vancomycin concentration independently estimated *via* competitive immunoassays (Fig. 5C). Given that these clinical samples contained vancomycin levels at or below 15 μM, a linear regression between E-AB *vs.* immunoassay measurements achieved a strong linear correlation coefficient of 0.94. Similarly, the corresponding Bland–Altman plot (Fig. 5D) indicated that the E-AB measurements displayed no over- or under-estimation bias across the population of samples. However, the data also shows significant scatter, which indicates that further optimization is needed for functional use of the 3D-printed E-AB sensor platform in clinical studies.

Extensive investigation of the source of this scatter led to the discovery that non-specific protein binding to the E-AB surface was at the source of the problem. Proteins from serum samples that adsorbed onto the E-AB sensor surface were not fully removed by mechanical polishing of the electrodes prior to sensor surface regeneration. To overcome this issue, we implemented a cleaning protocol based on electrochemical

roughening of the electrode surfaces as previously reported.[19] Briefly, after each use in serum samples, we first mechanically polished the 3D-printed devices, then conducted electrochemical roughening *via* voltage pulsing in 0.5 M H_2SO_4, cycling the voltage from 0 to 2 V for 20 ms, for a total of 16 000 cycles. This protocol caused the gold electrodes to change color from yellow to red, revealing the formation of nanofeatures on the gold surface, as previously reported. Modification of the device electrodes immediately after electrochemical roughening led to highly reproducible aptamer surface densities regardless of how many times the devices were recycled, with an approximately two-fold increase in packing density relative to unroughened electrodes (Fig. S5A†). Titrations performed using these sensors yielded more stable measurement values with less device-to-device and day-to-day variability (Fig. S4A and B†). Additionally, regression parameters for sensors fabricated using this new cleaning protocol, such as max/min gain and EC_{50}, were also more consistent (Fig. S5B–D†).

The results of electrochemically roughened sensors correlated better with the values returned by the immunoassay (Fig. 6A), with a slope near 1 and an R^2 value of 0.88 when plotted against each other and subjected to linear regression with the intercept constrained to zero. Additionally, the Bland–Altman plot (Fig. 6B) reveals that, while the mean difference value is slightly elevated compared to sensors on unroughened electrodes, the confidence interval is significantly smaller. Furthermore, we sought to confirm if multiple quantification uses in one E-AB sensing run affected the correlation with the immunoassay values. After separating the quantification values by their position in the measurement order (*i.e.* first measurements, second measurements, *etc.*), we see that the R^2 value for the linear regression decreases significantly after the second measurement (Fig. S6A–E†). This may indicate that multiple measurements, even with rinsing, slightly affect sensor performance. However, there is no significant difference in standard deviation between the first measurement and the subsequent measurements (Fig. S6F†).

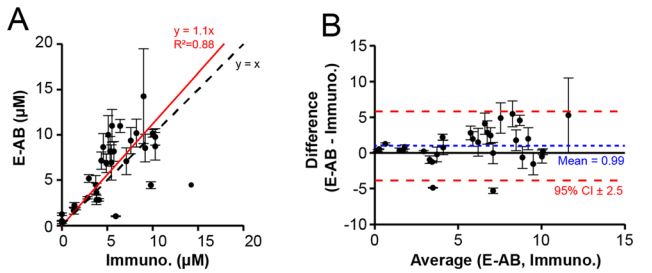

Fig. 6 Patient sample quantification with updated cleaning protocol. (A) Correlation between vancomycin concentrations calculated from E-AB sensor data (*y*-axis) and concentrations derived from competitive immunoassay results. The dashed black line represents a line of $y = x$, the solid red line represents the linear regression. Error bars represent standard deviation, $n = 3$ or 4 electrodes per point. (B) Bland–Altman plot of the patient sample data, with the difference between the values calculated from the E-AB sensor and immunoassay plotted as a function of the average of the two. The solid black line represents $y = 0$, the blue dashed line represents the mean difference value, and the red dashed lines represent the 95% confidence interval. Error bars represent standard deviation, $n = 3$ or 4 electrodes per point.

4. Conclusion

We report a method for constructing a stereolithographically 3D-printed device consisting of four gold electrode surfaces, a silver pseudo-reference electrode, and a platinum counter electrode, compatible with fabrication of electrochemical aptamer-based sensors. This device was assembled at relatively low cost, requiring only basic, widely available materials and access to an SLA printer. The convenience of the manufacturing approach makes it a potential alternative to commercial macroelectrodes, especially for labs who cannot afford the cost of obtaining the number of electrodes needed for statistically rigorous studies. The resin material used during cell prototyping could be changed according to preference or use-case; however, we note that the resin used in this study is specifically stable in the acidic and basic conditions required for electrochemical cleaning of the electrodes and does not appreciably absorb the sensor reagents or intended target. The devices reported in this work hold a small cell volume (75–300 μL), and four statistically redundant electrode channels, making them ideal for working with low volume biofluid samples, such as those obtained from biobanks. This is in contrast to using cMEs immersed in sample contained within a small vessel such as an Eppendorf tube, an approach that requires more volume of limited sample to achieve the same statistical redundancy (because of the need of working, counter and reference electrodes, plus replicate working electrodes) and requires considerable manual manipulation of the cell, which increases the risk of user exposure to any pathogens contained within the sample. Our multielectrode cell only requires pipetting sample in, minimizing sample manipulations.

We demonstrated that our devices were compatible with several different aptamer sequences, as well as with undiluted serum, a common biofluid used in patient sample analysis. It is important to note that, as with all electrodes, cleaning and pretreatment were extremely important in producing reproducible surfaces for E-AB sensor deposition. Performance of the sensors was vastly improved with more rigorous cleaning and surface roughening protocols. As seen in this study, more extensive cleaning and roughening allowed for a greater and more consistent packing density, leading to higher signal gain and better correlation with established quantification methods. Furthermore, quantification fidelity decreases with repeated use of an E-AB sensor, so future work should be aimed at extending this lifespan.

Data availability

Data will be openly available *via* a data repository, or from the corresponding author upon request.

Conflicts of interest

The authors declare no conflicts of interest.

Acknowledgements

This work was supported by the National Institute of General Medical Sciences of the National Institutes of Health under Award Number R01GM140143. The content is solely the responsibility of the authors and does not necessarily represent the official views of the National Institutes of Health.

References

1 A. Shaver, J. D. Mahlum, K. Scida, M. L. Johnston, M. Aller Pellitero, Y. Wu, G. V. Carr and N. Arroyo-Currás, Optimization of Vancomycin Aptamer Sequence Length Increases the Sensitivity of Electrochemical, Aptamer-Based Sensors In Vivo, *ACS Sens.*, 2022, **7**(12), 3895–3905, DOI: **10.1021/acssensors.2c01910**.

2 R. Y. Lai, K. W. Plaxco and A. J. Heeger, Aptamer-Based Electrochemical Detection of Picomolar Platelet-Derived Growth Factor Directly in Blood Serum, *Anal. Chem.*, 2007, **79**(1), 229–233, DOI: **10.1021/ac061592s**.

3 C. Parolo, A. Idili, G. Ortega, A. Csordas, A. Hsu, N. Arroyo-Currás, Q. Yang, B. S. Ferguson, J. Wang and K. W. Plaxco, Real-Time Monitoring of a Protein Biomarker, *ACS Sens.*, 2020, **5**(7), 1877–1881, DOI: **10.1021/acssensors.0c01085**.

4 Y. Yuan and N. Arroyo-Currás, Continuous Molecular Monitoring in the Body via Nucleic Acid–Based Electrochemical Sensors: The Need for Statistically-Powered Validation, *Curr. Opin. Electrochem.*, 2023, **39**, 101305, DOI: **10.1016/j.coelec.2023.101305**.

5 A. Sadana, Market Size and Economics for Biosensors, in *Fractal Binding and Dissociation Kinetics for Different Biosensor Applications*, Elsevier, 2005, pp. 265–299, DOI: **10.1016/B978-044451945-0/50014-5**.

6 Y. H. Chang, C. L. Hsu, C. J. Yuan, S. F. Tang, H. J. Chiang, H. Jang and K. S. Chang, Improvement of the Inter-Electrode Reproducibility of Screen-Printed Carbon Electrodes by Oxygen Plasma Etching and an Image Color Level Method for Quality Control, *Mater. Sci. Eng., C*, 2011, **31**(7), 1265–1270, DOI: **10.1016/j.msec.2011.01.001**.

7 R. García-González, M. T. Fernández-Abedul, A. Pernía and A. Costa-García, Electrochemical Characterization of Different Screen-Printed Gold Electrodes, *Electrochim. Acta*, 2008, **53**(8), 3242–3249, DOI: **10.1016/j.electacta.2007.07.059**.

8 S. K. Parupelli and S. Desai, A Comprehensive Review of Additive Manufacturing (3D Printing): Processes, Applications and Future Potential, *Am. J. Appl. Sci.*, 2019, **16**(8), 244–272, DOI: **10.3844/ajassp.2019.244.272**.

9 J. Wu, H. Liu, W. Chen, B. Ma and H. Ju, Device Integration of Electrochemical Biosensors, *Nat. Rev. Bioeng.*, 2023, **1**(5), 346–360, DOI: **10.1038/s44222-023-00032-w**.

10 I. Belmonte and R. J. White, 3-D Printed Microfluidics for Rapid Prototyping and Testing of Electrochemical, Aptamer-Based Sensor Devices under Flow Conditions, *Anal. Chim. Acta*, 2022, **1192**, 339377, DOI: **10.1016/j.aca.2021.339377**.

11 Y. Wu, F. Tehrani, H. Teymourian, J. Mack, A. Shaver, M. Reynoso, J. Kavner, N. Huang, A. Furmidge, A. Duvvuri, Y. Nie, L. M. Laffel, F. J. Doyle, M. E. Patti, E. Dassau, J. Wang and N. Arroyo-Currás, Microneedle Aptamer-Based Sensors for Continuous, Real-Time Therapeutic Drug Monitoring, *Anal. Chem.*, 2022, **94**(23), 8335–8345, DOI: **10.1021/acs.analchem.2c00829**.

12 J. N. Perry, A. Jasim, A. Hojat and W. H. Yong, Procurement, Storage, and Use of Blood in Biobanks, in *Methods in Molecular Biology*, Humana Press Inc., 2019, vol. 1897, pp. 89–97, DOI: **10.1007/978-1-4939-8935-5_9**.

13 N. Arroyo-Currás, J. Somerson, P. A. Vieira, K. L. Ploense, T. E. Kippin and K. W. Plaxco, Real-Time Measurement of Small Molecules Directly in Awake, Ambulatory Animals, *Proc. Natl. Acad. Sci. U. S. A.*, 2017, **114**(4), 645–650, DOI: **10.1073/pnas.1613458114**.

14 A. Shaver, N. Kundu, B. E. Young, P. A. Vieira, J. T. Sczepanski and N. Arroyo-Currás, Nuclease Hydrolysis Does Not Drive the Rapid Signaling Decay of DNA Aptamer-Based Electrochemical Sensors in Biological Fluids, *Langmuir*, 2021, **37**(17), 5213–5221, DOI: **10.1021/acs.langmuir.1c00166**.

15 S. D. Curtis, K. L. Ploense, M. Kurnik, G. Ortega, C. Parolo, T. E. Kippin, K. W. Plaxco and N. Arroyo-Currás, Open Source Software for the Real-Time Control, Processing, and Visualization of High-Volume Electrochemical Data, *Anal. Chem.*, 2019, **91**(19), 12321–12328, DOI: **10.1021/acs.analchem.9b02553**.

16 L. R. Schoukroun-Barnes, F. C. Macazo, B. Gutierrez, J. Lottermoser, J. Liu and R. J. White, Reagentless, Structure-Switching, Electrochemical Aptamer-Based Sensors, *Annu. Rev. Anal. Chem.*, 2016, 163–181, DOI: **10.1146/annurev-anchem-071015-041446**.

17 D. Giavarina, Understanding Bland Altman Analysis, *Biochem. Med.*, 2015, **25**(2), 141–151, DOI: **10.11613/BM.2015.015**.

18 Y. Liu, J. O. Mack, M. Shojaee, A. Shaver, A. George, W. Clarke, N. Patel and N. Arroyo-Currás, Analytical Validation of Aptamer-Based Serum Vancomycin Monitoring Relative to Automated Immunoassays, *ACS Sens.*, 2024, **9**(1), 228–235, DOI: **10.1021/acssensors.3c01868**.

19 N. Arroyo-Currás, K. Scida, K. L. Ploense, T. E. Kippin and K. W. Plaxco, High Surface Area Electrodes Generated via Electrochemical Roughening Improve the Signaling of Electrochemical Aptamer-Based Biosensors, *Anal. Chem.*, 2017, **89**(22), 12185–12191, DOI: **10.1021/acs.analchem.7b02830**.